Available online at www.sciencedirect.com
ScienceDirect
Biomaterials 28 (2007) 3306–3313
Biomaterials
www.elsevier.com/locate/biomaterials

Effects of calcium ion incorporation on bone healing of Ti6Al4V alloy implants in rabbit tibiae

Jin-Woo Park[a,*], Kwang-Bum Park[b], Jo-Young Suh[a]

[a]Department of Periodontology, School of Dentistry, Kyungpook National University, 188-1, Samduk 2Ga, Jung-Gu, Daegu 700 412, South Korea
[b]Mir Dental Hospital, 149-132, Samduk 2Ga, Jung-Gu, Daegu 700 412, South Korea

Received 7 February 2007; accepted 3 April 2007
Available online 10 April 2007

Abstract

The biocompatibility of calcium ion (Ca)-incorporated Ti6Al4V alloy implants, produced by hydrothermal treatment using a Ca-containing solution, was investigated. The surface characteristics were evaluated by scanning electron microscopy, thin-film X-ray diffractometry, Auger electron spectroscopy, and stylus profilometry. The viability of MC3T3-E1 cells on Ca-incorporated machined Ti6Al4V surfaces with different oxide thicknesses was compared with that on untreated machined Ti6Al4V surfaces with MTT assay. The osteoconductivity of the Ca-incorporated Ti6Al4V implants was evaluated by removal torque testing and histomorphometric analysis after 6 weeks of implantation in rabbit tibiae. Our results show that hydrothermal treatment with a Ca-containing solution produced a crystalline $CaTiO_3$ layer on Ti6Al4V surfaces, and calcium ions were gradually incorporated throughout the oxide layer. After immersion in Hank's balanced salt solution, a considerable apatite deposition was observed on all surfaces of the Ca-incorporated samples. Significant increases in cell viability ($p<0.001$), removal torque forces, and bone-to-implant contact values ($p<0.05$) were observed for Ca-incorporated Ti6Al4V implants compared with those for untreated Ti6Al4V implants.

Keywords: Titanium alloy; Calcium; Biocompatibility; Osseointegration; Histomorphometry; Cell viability

1. Introduction

Titanium (Ti) and Ti6Al4V (Ti64) alloy have been used as endosseous implant materials in dentistry and orthopedics because of their good mechanical properties and biocompatibility. However, because of their bioinertness, various surface treatments have been used to enhance bone healing around Ti implants. Numerous *in vitro* and *in vivo* studies have indicated the significant advantages of microrough-surfaced Ti implants in enhancing osseointegration. Implants with rough surfaces showed greater percentages of bone–implant contact and removal torque values than do those with relatively smooth, machined surfaces [1–3]. Osteoblastic cells cultured on roughened surfaces exhibit increases in osteoblast gene expression and mineralization compared with those on machined surfaces [4–6].

However, some concern has been raised about metal ion release from the surfaces of metallic implants, especially in those made of Ti6Al4V alloy. Aluminum and vanadium ions released from Ti6Al4V surfaces could impair normal bone healing processes, which would negatively affect osteoblast cell behavior [7–10]. Several *in vitro* studies have reported impaired cell adhesion, proliferation, and differentiation on rough Ti6Al4V alloy surfaces [11–13]. To increase the corrosion resistance and biocompatibility of Ti6Al4V alloy, many studies have focused on methods to control the crystallinity and thickness of the Ti oxide layer. It has been reported that a thick Ti oxide layer produced by thermal oxidation or anodic oxidation reduced metal ion release, which in turn improved the *in vitro* biocompatibility and bone formation of Ti6Al4V alloy implants [14–17].

Recently reported *in vitro* and *in vivo* studies have demonstrated the potential effectiveness of a calcium ion (Ca)-incorporated Ti oxide layer in enhancing osseointegration, Ca-incorporation enhanced attachment and

*Corresponding author. Tel.: +82 53 660 6913; fax: +82 53 427 3263.
E-mail address: jinwoo@knu.ac.kr (J.-W. Park).

0142-9612/$ - see front matter © 2007 Elsevier Ltd. All rights reserved.
doi:10.1016/j.biomaterials.2007.04.007

proliferation of osteoblastic cells and bone formation of Ti implants [18–20]. Recently, we reported that a Ti oxide layer with Ca-incorporation, produced by hydrothermal treatment, significantly increased the bone–implant contact and the removal torque force of commercially pure Ti implants with blasted surface in rabbit tibiae [21]. We found that a Ca-incorporated Ti oxide layer ($CaTiO_3$), produced by hydrothermal treatment using a mixed solution of sodium hydroxide (NaOH) and calcium oxide (CaO), preserved the original microtopographies of grit-blasted Ti surfaces. It is expected that a thick oxide layer with a biologically active composition (calcium chemistry) may improve the biocompatibility of Ti6Al4V alloy implants by enhancing osteoblast response and bone response.

Therefore, we evaluated the biocompatibility of Ca-incorporated Ti6Al4V alloy implants produced by hydrothermal treatment for future biomedical use. For this purpose, the surface characteristics and cell viability of Ca-incorporated Ti6Al4V alloy were investigated and its osteoconductivity was evaluated by removal torque testing and histomorphometric analysis after 6 weeks of implantation in rabbit tibiae.

2. Materials and methods

2.1. Sample preparation

Two different sample shapes, made from commercial Ti6Al4V (Ti64) plate with a thickness of 1 mm, were used to characterize the surface and evaluate cell viability. Square Ti64 samples ($10 \times 10 \times 1$ mm) were used for surface characterization. For the cell experiments, 6 mm diameter Ti64 disks were used. The samples were abraded under wet conditions to 1200 grit SiC abrasive paper and successively cleaned in acetone, alcohol, and deionized water (Ti64–0). They were then further treated to produce calcium titanate ($CaTiO_3$) layers of different thicknesses with a hydrothermal treatment, as in author's previous studies [21,22]. Briefly, Ti64 samples were treated in a Ca-containing solution (mixed solution of CaO and NaOH dissolved in deionized water) as follows: (1) treated in a mixed solution of 0.1 M NaOH and 2 mM CaO at 180 °C for 24 h (Ti64–0.1); (2) treated in a mixed solution of 0.2 M NaOH and 2 mM CaO at 180 °C for 24 h (Ti64–0.2); and (3) treated in a mixed solution of 0.5 M NaOH and 2 mM CaO at 180 °C for 24 h (Ti64–0.5). After treatment, the samples were ultrasonically cleaned in deionized water and air dried. All samples were sterilized by γ-irradiation before the cell culture experiment.

For the animal study, screw-type implants ($n = 48$) with an external diameter of 2.4 mm and a length of 8 mm, made of commercial Ti64 alloy, with machined surfaces (machined implants) were purchased (JEIL Medical Co., Seoul, Korea). The Ca-incorporated implants were prepared under a hydrothermal condition as used to produce the Ti64–0.2 samples (Ca implants). This condition has been shown in a previous study to enhance bone healing around commercially pure Ti implants in rabbit tibiae [21]. All implants were cleaned and sterilized in the manner described above.

2.2. Surface characterization

The surface morphology of the Ti64 plates and implants was observed by scanning electron microscopy (SEM; S-4300, Hitachi, Tokyo, Japan). The crystalline structure and chemical composition of the TiO_2 layer were evaluated by thin-film X-ray diffractometry (XRD; X'Pert-APD, Philips, Netherlands) and Auger electron spectroscopy (AES; PHI 680 Auger Nanoprobe, Physical Electronics, USA) using Ti64 plates. Surface roughness measurements of the Ti64 plates were made with stylus profilometry (Form Talysurf Series 2, Taylor Hobson, London, UK); five samples from each group were measured, and two measurements were performed on each sample to evaluate the average surface roughness (R_a) values. The R_a value of the screw implants was measured by optical profilometry (WYKO NT 2000, Veeco Instruments Inc., Woodbury, NY, USA); two implants from each group were measured and three measurements were performed on the thread valley. The thickness of the Ca-incorporated Ti oxide layer was determined from the depth of the window formed after sputtering, leaving a step in the surface. This step was measured with a profilometer.

2.3. Evaluation of the in vitro bioactivity of the treated samples

To evaluate the apatite-forming ability of the treated samples, Ti64 plates were immersed vertically in 20 mL of Hank's balanced salt solution (HBSS; Cambrex Bioscience Inc., Walkersville, MD, USA, Ref. 10-527F) in a Teflon-sealed bottle at pH 7.4 and 37 °C. The solution was changed every 3 days. After immersion, the Ti plates were washed in distilled water and then air dried.

2.4. Cell culture and cell viability

MC3T3-E1 cells, a mouse calvaria-derived osteoblast-like cell line, were plated in Dulbecco's modified Eagle's medium (Gibco BRL Life Technologies, Grand Island, NY, USA) containing 10% fetal bovine serum (Gibco BRL Life Technologies), 500 units/mL penicillin (Keunhwa Pharmaceutical Co., Seoul, Korea), and 500 units/mL streptomycin (Donga Pharmaceutical Co., Seoul, Korea). The cells were cultured in an atmosphere of 100% humidity, 5% CO_2, and 37 °C. The medium was changed every other day until the cells reached confluence. When the cells reached confluence, they were passaged using 0.05% trypsin/0.02% EDTA.

Cell viability was measured with a 3-(4,5-dimethylthiazol-2yl)-2,5-diphenyl tetrazolium bromide (MTT) assay on four groups of Ti64 disks (6 mm diameter) with different surfaces. MTT is transformed by mitochondrial dehydrogenases into formazan, allowing cell viability and proliferation to be assessed [23]. The cells were seeded on Ti64 disks in 96-well cell culture plates at a density of 2000 cells/well and cultured for 1 and 4 days. Then, 50 μL of MTT solution prewarmed to 37 °C was added to each well and culture continued for 3 h under the same condition. The reaction was stopped by the addition of 200 μL of dimethylsulfoxide and 50 μL of glycine buffer to each well. The solutions were then transferred to new wells and the absorbance was measured at a wavelength of 570 nm using an ELISA plate reader (Precision Microplate Reader; Molecular Devices, Sunnyvale, CA, USA).

2.5. Animals and surgical procedure

Seven adult male New Zealand White rabbits weighing 3.5–4.0 kg were used in this study. This experiment was approved by the Institutional Animal Care and Use Committee of Kyungpook National University Hospital, Daegu, Korea. General anesthesia was induced by intramuscular injection of a combination of 1.3 mL of ketamine (100 mg/mL; Ketara, Yuhan, Seoul, Korea) and 0.2 mL of xylazine (7 mg/kg body weight; Rompun, Bayer Korea, Seoul, Korea). The medial surfaces of the proximal tibiae were used as the surgical sites. The surgical areas were shaved and the skin was washed with a mixture of iodine and 70% ethanol before surgical draping. Local anesthesia was induced with 1.0 mL of 2% lidocaine (1:100,000 epinephrine; Yuhan, Seoul, Korea) to control bleeding and to provide additional local anesthesia. The surgical sites were exposed with an incision through the skin, fascia, and periosteum at the medial surface of the proximal tibiae using sterile surgical techniques.

The implant site osteotomies were prepared in the usual manner. A final drill diameter of 2 mm was used. All drilling procedures were carried

out under profuse sterile saline irrigation. Six screw-shaped implants were placed in one animal; a set of three control implants and a set of three experimental implants were randomly placed in the right and left rabbit tibiae. Machined control implants ($n = 21$) and Ca-incorporated experimental implants ($n = 21$) were inserted with self-tapping until the implants were in their final positions, in which the top surface of the implant was in a position 1.5 mm above the cortical bone surface. All implants penetrated the first bone cortex only.

After surgery, the surgical sites were closed in layers and sutured using Vicryl (Ethicon, Somerville, NJ, USA). Antibiotics (Baytril, Bayer Korea) and analgesics (Nobin, Bayer Korea) were injected intramuscularly for 3 days to prevent postsurgical infection and to control pain. The animals were killed by intravenous injections of air under general anesthesia 6 weeks after surgery. Tissues were taken for removal torque tests and histomorphometric evaluation.

2.6. Removal torque tests

Removal torque tests were performed to evaluate implant stability in the bone bed. The removal torque value in Newton centimeters (Ncm) reflects the interfacial shear strength [24]. Two of the distal implants from each leg were subjected to removal torque testing (seven rabbits; Ca implants, $n = 14$; machined implants, $n = 14$). The proximal tibiae containing the implants were removed *en bloc*. They were firmly stabilized with a locking vise and the peak removal torque force was measured using a digital torque meter (MG series, Mark-10 Corporation, New York, NY, USA) with a measuring range of 0–14 Ncm. A single blinded examiner recorded all measurements of the peak torque to initiate reverse rotation.

2.7. Specimen preparation and histomorphometric evaluation

The most proximal implant in each leg was selected for histomorphometric evaluation. The proximal tibiae containing the implants were removed *en bloc*, fixed in 4% neutral buffered formaldehyde, dehydrated using an ascending series of alcohols, and embedded in methyl methacrylate for undecalcified sectioning. Undecalcified cut-and-ground sections, which were prepared in a plane parallel to the long axis of each implant and containing the central part of the implants, were produced at a final thickness of 20 μm using a Macro cutting and grinding system (Exakt 310 CP series, Exakt Apparatebau, Norderstedt, Germany). The sections were stained with Villanueva stain, and histomorphometric analysis was carried out using a light microscope (BX51, Olympus, Tokyo, Japan) with an image analysis system (i-Solution, iMTechnology Inc., Daejeon, Korea) under $\times 100$ magnification. The images were captured using a digital camera (CC-12, Soft Imaging System GmbH, Munster, Germany) attached to the microscope and displayed on a computer monitor. The percentage of bone-to-implant contact (BIC%) over the total length of the implant was measured (seven rabbits; Ca implants, $n = 7$; machined implants, $n = 7$). BIC% was measured as the percentage of the length of mineralized bone in direct contact with the implant surface.

2.8. Statistical analysis

Statistical analysis was performed using the SAS statistical system (SAS Institute, Cary, NC, USA). The means and standard deviations of cell viability, removal torque values and BIC% were calculated. One-way analysis of variance with Tukey's multiple comparisons test was performed to evaluate differences in cell viability between all groups. The paired Student t-test was performed to compare the values of removal torque force and BIC% between implants from left and right tibiae. Values of p less than 0.05 were considered statistically significant.

3. Results

3.1. Surface characteristics

SEM observation at a magnification of $\times 1000$ showed Ca-incorporated Ti64 surfaces had the original surface morphologies and typical anisotropic abrasive marks produced by abrasion after hydrothermal treatment (Fig. 1),

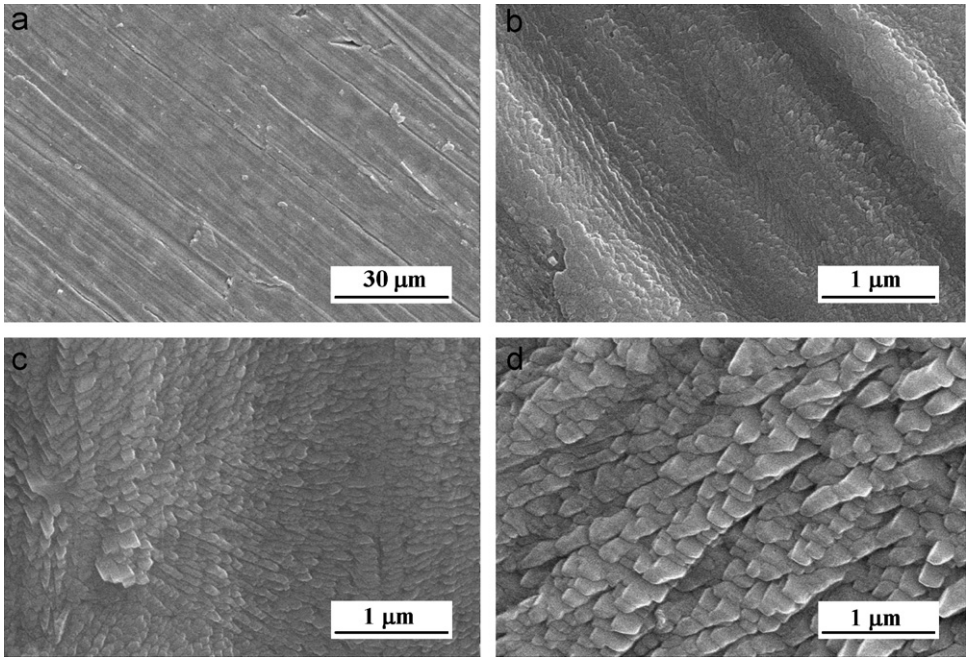

Fig. 1. Scanning electron microscope images of Ca-incorporated Ti6Al4V samples. (a) Ti6Al4V–0.2, (b) Ti6Al4V–0.1, (c) Ti6Al4V–0.2, and (d) Ti6Al4V–0.5 at magnifications of $\times 1000$ (a) and $\times 30{,}000$ (b–d). SEM image shows that Ca-incorporated Ti6Al4V surface preserves the original micron-scale morphology with typical anisotropic abrasive marks caused by machining at a magnification of $\times 1000$ (a). Nanostructure formation can be seen on the surfaces of Ca-incorporated Ti6Al4V surfaces at a higher magnification (b–d).

but the Ti64–0.5 samples exhibited accentuated grain structures because of the strong etching and accelerated crystalline $CaTiO_3$ growth resulting from the high concentration of NaOH (not shown). At a higher magnification (× 30,000), the surface nanostructure was observed on the surfaces of Ca-incorporated Ti64 substrates and screw implants (Figs. 1 and 2). Surface roughness measurements showed similar R_a values in all groups of Ti64 plates (Table 1). The control and experimental screw implants had similar R_a values (0.37 μm for machined implants and 0.35 μm for Ca implants). XRD analysis showed the formation of a crystalline $CaTiO_3$ (JCPDS #22-0153) surface layer in the hydrothermally treated Ti64 samples. The crystallinity and thickness of the $CaTiO_3$ layer increased with an increasing concentration of NaOH (Figs. 3 and 4). The AES depth profile showed a graded surface structure of the Ca-incorporated Ti oxide layer (Fig. 4). The thickness of the Ca-incorporated Ti oxide layers of Ti64−0.1, Ti64−0.2, and Ti64−0.5 were approximately 250, 500, and 1200 nm, respectively, as determined by profilometry.

3.2. Apatite precipitation on Ca-incorporated Ti samples

After the Ti64 samples had been soaked in HBSS, considerable apatite was formed on all the surfaces of the Ca-incorporated samples (Fig. 5).

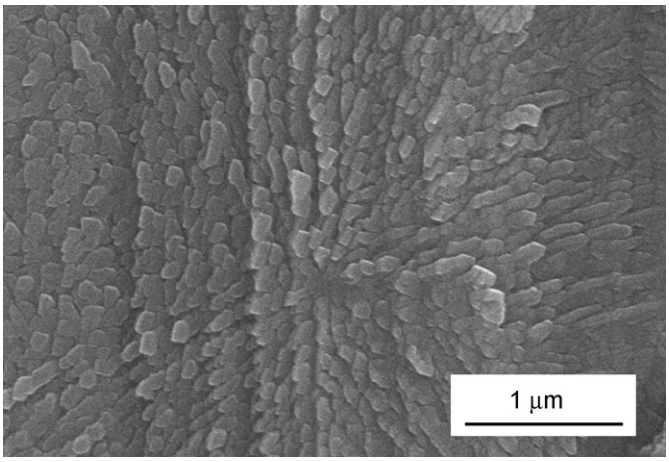

Fig. 2. Scanning electron microscope image of Ca-incorporated Ti6Al4V screw implant at a magnification of × 30,000.

3.3. Cell viability

MTT-based assay was used to investigate the mitochondrial functions of cultured osteoblasts on the different Ti64 surfaces. Fig. 6 shows the results of the MTT assay. The average absorbance values were expressed as a percentage of the control, Ti64−0 (absorbance value at day 1). Osteoblasts cultured on Ca-incorporated Ti64 surfaces showed significantly higher absorbance compared with that of cells on the untreated Ti64 surface (Ti64−0) at 4 days of culture ($p < 0.001$).

3.4. Removal torque testing

The Ca implants showed mean removal torque value significantly higher than that of the machined implants (3.2 ± 1.2 vs. 2.2 ± 0.9 Ncm, respectively; $p < 0.05$).

3.5. Histological evaluation and bone-to-implant contact percentages (BIC%)

Six weeks after implantation, all implants in the control and experimental groups were histologically in direct contact with the surrounding cortical bone along their

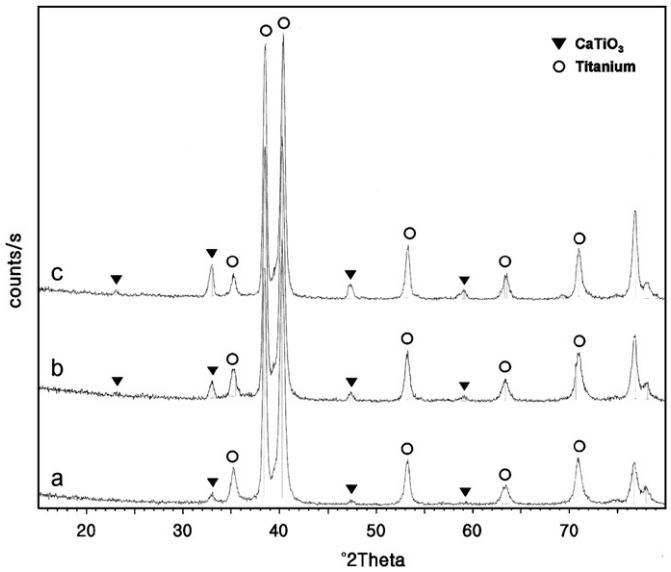

Fig. 3. X-ray diffraction patterns of Ti6Al4V–0.1 (a), Ti6Al4V–0.2 (b), and Ti6Al4V–0.5 (c) samples.

Table 1
Average surface roughness values (R_a) of Ti6Al4V surfaces (mean ± SD; $n = 10$)

Group	R_a (μm)
Ti6Al4V−0	0.29 ± 0.04
Ti6Al4V−0.1	0.27 ± 0.02
Ti6Al4V−0.2	0.31 ± 0.05
Ti6Al4V−0.5	0.42 ± 0.07

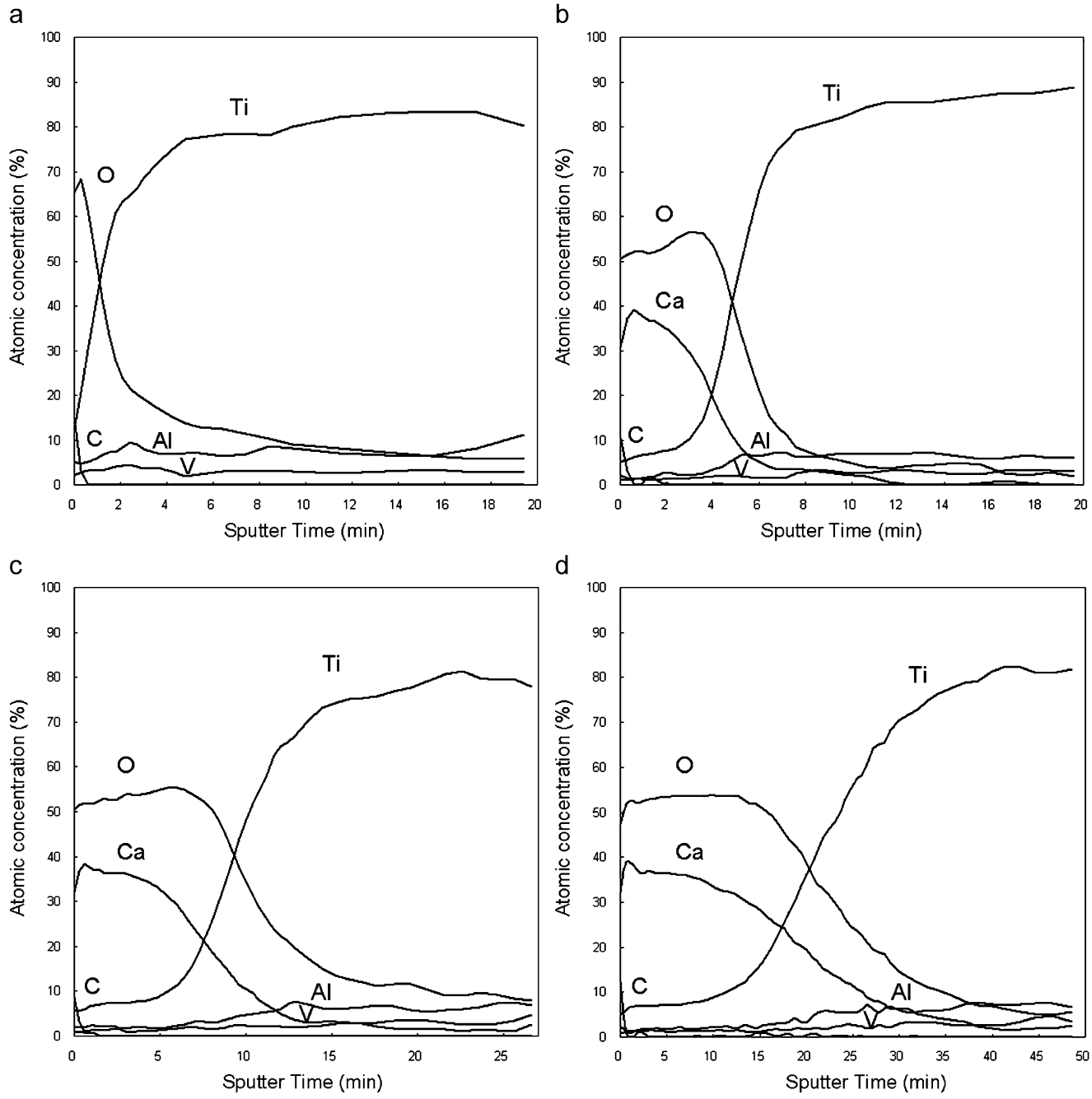

Fig. 4. Auger electron spectroscopy depth profiles of Ti6Al4V–0 (a), Ti6Al4V–0.1 (b), Ti6Al4V–0.2 (c), and Ti6Al4V–0.5 (d) samples.

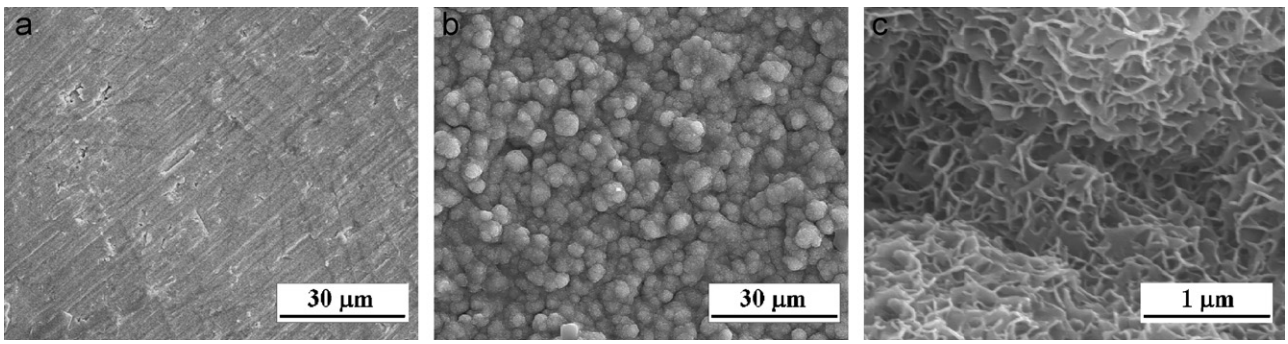

Fig. 5. Scanning electron microscope images of Ti6Al4V samples soaked in HBSS for 4 weeks. (a) Ti6Al4V–0 and (b and c) Ti6Al4V–0.2 samples at magnifications of $\times 1000$ (a and b) and $\times 30{,}000$ (c). Ti6Al4V–0.2 samples show the formation of a thick apatite layer on their surfaces (b and c).

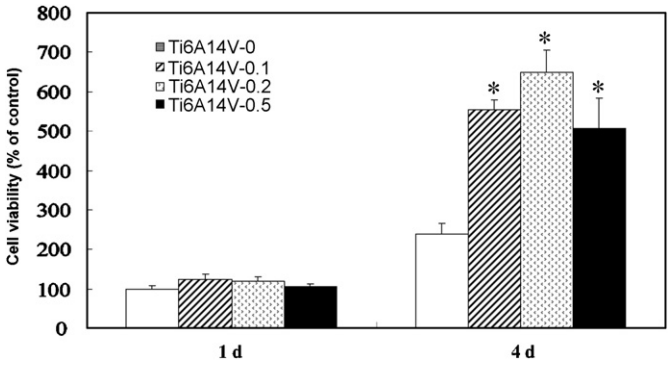

Fig. 6. Cell viability expressed as a percentage of the viability of cells on untreated Ti6Al4V after 1 and 4 days of culture on Ca-incorporated Ti6Al4V samples. Data are reported as means ± SD ($n = 5$ per group). *$p < 0.001$ compared to untreated Ti6Al4V surfaces.

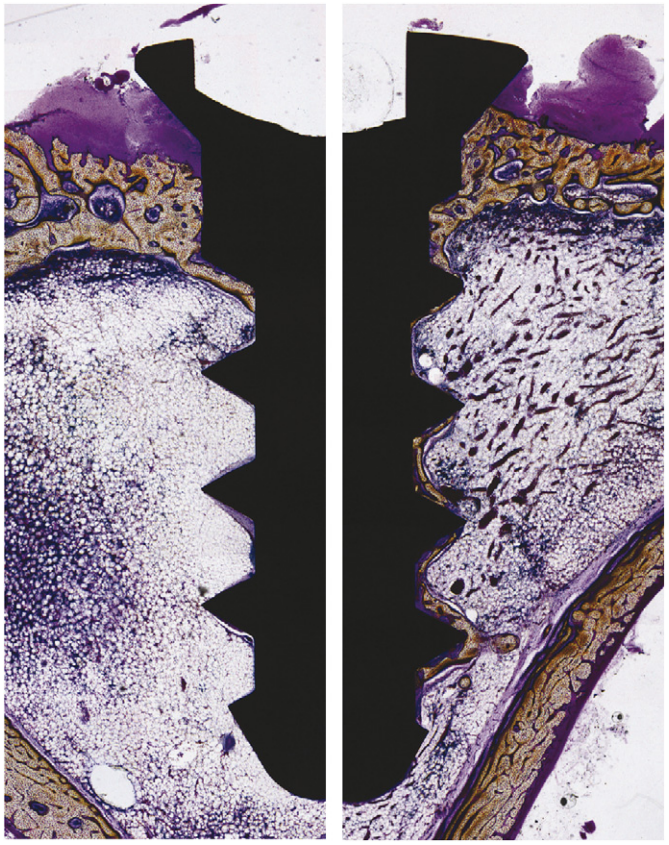

Fig. 7. Histological sections of machined (left) and Ca-incorporated (right) implants 6 weeks after implantation in rabbit tibiae. The Ca implant shows a higher degree of bone–implant contact in the medullary canal, which is devoid of surrounding bone, compared with that of the machined implant (stained with Villanueva stain).

upper threads (Fig. 7). The Ca implants showed more active bone formation in the medullary canal compared with that of the machined implants. The mean BIC% over the total implant length was 20.2 ± 13.0% for the machined implants, and 36.7 ± 9.2% for the Ca implants, and the difference between the two groups was statistically different ($p < 0.05$).

4. Discussion

The results of this study demonstrate that the biocompatibility of Ti6Al4V alloy can be improved by a Ca-incorporated oxide layer. Ca-incorporated Ti64 surfaces showed considerable apatite formation after they were soaked in HBSS. It has been suggested that the *in vitro* apatite-forming ability of Ti surfaces in simulated body fluid is consistent with the *in vivo* bone-bonding behavior of implants and that apatite formation is the decisive factor in osseointegration [25–27]. Calcium ions in the $CaTiO_3$ layer may play a role in apatite formation because a greater number of phosphate ions can be adsorbed to the Ca-incorporated surface, resulting in the acceleration of calcium phosphate formation, as suggested by Hanawa et al. [28,29]. In this study, the presence of relatively large amounts of calcium ions (approximately 40% at the outer surface) on the Ti64 surface may have contributed to the acceleration of apatite formation. Moreover, it seems that the surface nanostructure of hydrothermally treated Ti64 provides more nucleation sites for apatite formation.

Osteoblasts grown on Ca-incorporated Ti64 surfaces with various thicknesses of Ti oxide exhibited cell viability significantly greater than that of cells on unmodified Ti64 surfaces. It can be assumed that the abundant calcium ions incorporated into the relatively thick Ti oxide layer (250–1200 nm in thickness) produced by the hydrothermal treatment contributed to the increased cell viability by stimulating integrin-mediated osteoblast response through enhanced ligand binding of the integrin receptor [18,19,30,31]. The increased cell viability on Ca-incorporated Ti6Al4V surfaces is somewhat in accordance with recently reported studies showing enhanced osteoblast adhesion, spreading, and growth on Ca-incorporated Ti surfaces [18,19,32]. It has been reported that, at physiological pH, the Ca component increases protein adsorption, extracellular matrix (ECM) proteins containing RGD sequence that promotes cell attachment, onto the Ti surfaces by ionic bonding, which may subsequently affect cell responses [33–35]. Feng et al. [35] reported enhanced adsorption of fibronectin and vitronectin, important cell adhesive proteins containing RGD sequence, onto Ca sites on material surfaces. Studies have indicated the enhanced osteoblast adhesion and spreading mediated by RGD domain of fibronectin and vitronectin as a possible reason for the osteoconductivity of materials [36,37]. Nayab et al. [19] reported that Ca-implantation into Ti dose-dependently enhanced the quality of attachment and spreading of MG-63 cells. They found significant increases in $\alpha 5\beta 1$ integrin expression in cells grown on Ti surfaces with high levels of Ca after 24 h of culture. Therefore, it may be assumed that acceleration in the early osteoblast response contributed to an improvement in subsequent cell viability. For these reasons, it can be inferred that an abundant Ca component in the outer oxide layer enhanced cell attachment and proliferation, which in turn resulted in enhanced bone healing in this study. In addition, the surface

nanostructure may be another possible reason for enhanced osteoconductivity of Ca-incorporated Ti64 implants, which might increase the reactivity of Ca-incorporated surface by increasing its surface area exposed to the biological environment. However, further detailed *in vitro* studies are required to clarify osteoblast behaviors on Ca-incorporated Ti6Al4V surfaces produced by hydrothermal treatment.

In this study, the effect of Ca incorporation on the osteoconductive properties of Ti64 alloy implants was investigated by comparing the bone–implant contact and removal torque force of a Ca-incorporated Ti64 surface with those of unmodified machined Ti64 surface. Statistically significant differences in BIC% and removal torque values were found between the machined and the Ca implants, despite similar values for average surface roughness (R_a) in the two groups. The surface of the Ca implant exhibited higher bone-to-implant contact, suggesting that the calcium chemistry, provided by $CaTiO_3$, enhances bone formation around Ti64 implants. The higher BIC% for the Ca implant originated from the greater degree of bone contact with the implant surfaces in the medullary canal of rabbit tibia, which is characterized by an absence of cancellous bone, indicating the improved osteoconductive properties of Ca-incorporated implant. These results are consistent with those of other *in vivo* studies in which Ca-deposited Ti implants, prepared by ion implantation or anodic oxidation, achieved fast and strong osseointegration [20,38,39]. These results also confirm our previous *in vivo* study, which reported that a $CaTiO_3$ layer produced by hydrothermal treatment enhanced the osteoconductivity of commercially pure Ti implants with microrough surfaces [21]. We have shown that, in contrast to calcium phosphate coatings such as plasma-sprayed hydroxyapatite coating, this Ca-incorporated Ti oxide layer ($CaTiO_3$) produced by hydrothermal treatment has good mechanical properties and provides Ti implants with bioactivity [21].

This Ca-incorporated surface offers a cytocompatible surface for osteoblasts and enhances the osteoconductivity of machined Ti6Al4V implants in rabbit tibiae. The mechanism of effect is likely to be via enhanced adsorption of RGD containing ECM proteins and acceleration of integrin-mediated osteoblast responses on Ca-incorporated Ti64 implants with a greater surface area provided by their surface nanostructures.

5. Conclusions

Our results show that the Ca-incorporated Ti oxide layer ($CaTiO_3$), produced by hydrothermal treatment using a mixed solution of NaOH and CaO, may be an effective tool for the improvement of the biocompatibility of Ti6Al4V implants. However, further detailed studies are needed to better understand the effects of this type of Ca-incorporated surface on osteoblast responses and bone responses.

Acknowledgments

This work was supported by a Biomedical Research Institute grant, Kyungpook National University Hospital (2006).

References

[1] Buser D, Nydegger T, Oxland T, Cochran DL, Schenk RK, Hirt HP, et al. Interface shear strength of titanium implants with a sandblasted and acid-etched surface: a biomechanical study in the maxilla of miniature pigs. J Biomed Mater Res 1999;45:75–83.

[2] Godfredsen K, Nimb L, Hjorting-Hansen E, Jensen JS, Holmen A. Histomorphometric and removal torque analysis for TiO_2-blasted titanium implants. An experiment on dogs. Clin Oral Implants Res 1992;77–84.

[3] Trisi P, Lazzara R, Rao W, Rebaudi A. Bone-implant contact and bone quality: evaluation of expected and actual bone contact and machined and osseotite implants surfaces. Int J Periodont Restorat Dent 2002;22:535–45.

[4] Marinucci L, Balloni S, Becchetti E, Belcastro S, Guerra M, Calvitti M, et al. Effect of titanium surface roughness on human osteoblast proliferation and gene expression *in vitro*. Int J Oral Maxillofac Implants 2006;21:719–25.

[5] Masaki C, Schneider GB, Zaharias R, Seabold D, Stanford C. Effects of implant surface microtopography on osteoblast gene expression. Clin Oral Implants Res 2005;16:650–6.

[6] Schneider GB, Perinpanayagam H, Clegg M, Zaharias R, Seabold D, Keller J, et al. Implant surface roughness affects osteoblast gene expression. J Dent Res 2003;82:372–6.

[7] Hallab NJ, Vermes C, Messina C, Roebuck KA, Glant TT, Jacobs JJ. Concentration- and composition-dependent effects of metal ions on human MG-63 osteoblasts. J Biomed Mater Res 2002;60:420–33.

[8] Sun ZL, Wataha JC, Hanks CT. Effects of metal ions on osteoblast-like cell metabolism and differentiation. J Biomed Mater Res 1997;34:29–37.

[9] Thompson GJ, Puelo DA. Ti-6Al-4V ion solution inhibition of osteogenic cell phenotype as a function of differentiation time course *in vitro*. Biomaterials 1996;17:1949–54.

[10] Wang JY, Wicklund BH, Gustilo RB, Tsukayama DT. Prosthetic metals interfere with the functions of human osteoblast cells *in vitro*. Clin Orthop Relat Res 1997;339:216–26.

[11] Eisenbarth E, Meyle J, Nachtigall W, Breme J. Influence of the surface structure of titanium materials on the adhesion of fibroblasts. Biomaterials 1996;17:1399–403.

[12] Lincks J, Boyan BD, Blanchard CR, Lohmann CH, Liu Y, Cochran DL, et al. Response of MG63 osteoblast-like cells to titanium and titanium alloy is dependent on surface roughness and composition. Biomaterials 1998;19:2219–32.

[13] Spyrou P, Papaioannou S, Hampson G, Brady K, Palmer RM, McDonald F. Cytokine release by osteoblast-like cells cultured on implant discs of varying alloy compositions. Clin Oral Implants Res 2002;13:623–30.

[14] Garcia-Alonso MC, Saldana L, Valles G, Gonzalez-Carrasco JL, Gonzalez-Cabrero J, Martinez ME, et al. *In vitro* corrosion corrosion behavior and osteoblast response of thermally oxidized Ti6Al4V alloy. Biomaterials 2003;24:19–26.

[15] MacDonald DE, Rapuano BE, Deo N, Stranick M, Somasundaran P, Boskey AL. Thermal and chemical modification of titanium-aluminum-vanadium implant materials: effects on surface properties, glycoprotein adsorption, and MG63 cell attachment. Biomaterials 2004;25:3135–46.

[16] Saldana L, Vilaboa N, Valles G, Gonzalez-Cabrero J, Munuera L. Osteoblast response to thermally oxidized Ti6Al4V alloy. J Biomed Mater Res A 2005;73:97–107.

[17] Yamagami A, Yoshihara Y, Suwa F. Mechanical and histologic examination of titanium alloy material treated by sandblasting and anodic oxidation. Int J Oral Maxillofac Implants 2005;20:48–53.
[18] Nayab SN, Jones FH, Olsen I. Human alveolar bone cell adhesion and growth on ion-implanted titanium. J Biomed Mater Res A 2004;69:651–7.
[19] Nayab SN, Jones FH, Olsen I. Effects of calcium ion implantation on human bone cell interaction with titanium. Biomaterials 2005;26: 4717–27.
[20] Sul YT, Johansson CB, Albrektsson T. Oxidized titanium screws coated with calcium ions and their performance in rabbit bone. Int J Oral Maxillofac Implants 2002;17:625–34.
[21] Suh J-Y, Jeung O-C, Choi B-J, Park J-W. Effects of a novel calcium titanate coating on the osseointegration of blasted endosseous implants in rabbit tibiae. Clin Oral Implants Res, doi:10.1111/j.1600-0501.2006.01323.x.
[22] Park J-W. Electrolyte solution for implant surface treatment, method for implant surface treatment using the same, and implant manufactured by the same. KR Patent No. 100611945, 2006.
[23] Mossman T. Rapid colorimetric assay for cellular growth and survival: a application to proliferation and cytotoxicity assays. J Immunol Methods 1983;65:55–63.
[24] Johansson CB, Han CH, Wennerberg A, Albrektsson T. A quantitative comparison of machined commercially pure titanium and titanium–aluminum–vanadium implants in rabbit bone. Int J Oral Maxillofac Implants 1998;13:315–21.
[25] Wang XX, Yan W, Hayakawa S, Tsuru K, Osaka A. Apatite deposition on thermally and anodically oxidized titanium surfaces in a simulated body fluid. Biomaterials 2003;24:4631–7.
[26] Xue W, Liu X, Zheng X, Ding C. *In vivo* evaluation of plasma-sprayed wollastonite coating. Biomaterials 2005;26:3455–60.
[27] Yan WQ, Nakamura T, Kobayashi M, Kim HM, Miyaji F, Kokubo T. Bonding of chemically treated titanium implants to bone. J Biomed Mater Res 1997;37:267–75.
[28] Hanawa T, Ukai H, Murakami K. X-ray photoelectron spectroscopy of calcium-ion-implanted titanium. J Electron Spectrosc Relat Phenom 1993;63:347–54.
[29] Hanawa T, Kon M, Doi H, Ukai H, Murakami K, Hamanaka H, et al. Amount of hydroxyl radical on calcium-ion-implanted titanium and point of zero charge of constituent oxide of the surface-modified layer. J Mater Sci Mater Med 1998;9: 89–92.
[30] Ajroud K, Sugimori T, Goldmann WH, Fathallah DM, Xiong JP, Arnaout MA. Binding affinity of metal ions to the CD11b A-domain is regulated by integrin activation and ligands. J Biol Chem 2004;279:25483–8.
[31] Shah AK, Lazatin J, Sinha RK, Lennox T, Hickok NJ, Tuan RS. Mechanism of BMP-2 stimulated adhesion of osteoblastic cells to titanium alloy. Biol Cell 1999;91:131–42.
[32] Webster TJ, Ergun C, Doremus RH, Lanford WA. Increased osteoblast adhesion on titanium-coated hydroxyapatite that forms $CaTiO_3$. J Biomed Mater Res A 2003;67:975–80.
[33] Ellingsen JE. A study on the mechanism of protein adsorption to TiO_2. Biomaterials 1991;12:593–6.
[34] Klinger A, Steinberg D, Kohavi D, Sela MN. Mechanism of adsorption of human albumin to titanium *in vitro*. J Biomed Mater Res 1997;36:387–92.
[35] Feng B, Weng J, Yang BC, Qu SX, Zhang XD. Characterization of titanium surfaces with calcium and phosphate and osteoblast adhesion. Biomaterials 2004;25:3421–8.
[36] Matsuura T, Hosokawa R, Okamoto K, Kimoto T, Akagawa Y. Diverse mechanisms of osteoblast spreading on hydroxyapatite and titanium. Biomaterials 2000;21:1121–7.
[37] Webster TJ, Ergun C, Doremus RH, Siegel RW, Bizios R. Specific proteins mediate enhanced osteoblast adhesion on nanophase ceramics. J Biomed Mater Res 2000;51:475–83.
[38] Jinno T, Kirk SK, Morita S, Goldberg VM. Effects of calcium ion implantation on osseointegration of surface blasted titanium alloy femoral implants in a canine total hip arthroplasty model. J Arthroplasty 2004;19:102–9.
[39] Sul YT. The significance of the surface properties of oxidized titanium to the bone response: special emphasis on potential biochemical bonding of oxidized titanium implant. Biomaterials 2003;24:3893–907.